Experimental Techniques
https://doi.org/10.1007/s40799-023-00645-1

RESEARCH PAPER

Balancing Impedance and Controllability in Response Reconstruction with TS-IMMAT

M. J. Tuman[1] · M. Behling[2] · M. S. Allen[2] · W. J. DeLima[3] · J. Hower[3] · R. L. Mayes[4]

Received: 29 December 2022 / Accepted: 16 March 2023

Abstract

In a prior work the authors proposed a variant on the Impedance Matched Multi-Axis Test (IMMAT) in which a fixture is defined, called the Transmission Simulator (TS), and the desired environment is matched at a set of sensors on the TS. If the motion of the TS is matched then the response of the rest of the component will also match, provided that the attached component has the same dynamics as it did when the environment was measured. Hence, one would like the TS to be flexible so that it reproduces the boundary conditions that the component of interest experiences during flight, but the more flexible the TS, the more shakers might be needed to control its response. This work presents a derivation that gives expressions for these two potential error sources in TS-IMMAT. Then, various case studies are presented, both on simulated and real hardware, to understand the importance of each error term in practical testing. The theory explains the phenomena that were observed when using measurements from a component that flew on a sounding rocket. The environmental response was measured and then various fixtures were attached, each comprising more of the next assembly, or the hardware to which the component was attached in flight. MIMO testing was repeated with each fixture and the results were compared to seek to understand the role of the impedance match in this type of testing. The results show that the number of modes that are active in the transmission simulator is also very important, and so the best solution balances these two considerations. An improved method of simulating the MIMO test is then proposed, so simulations can be used to predict what fixture, or transmission simulator, will give the best results in a TS-IMMAT test.

Keywords Shaker Test · Operational Vibration Environment · Substructuring · Force Reconstruction

✉ M. J. Tuman
tuman@wisc.edu

M. Behling
mebehlin@student.byu.edu

M. S. Allen
matt.allen@byu.edu

W. J. DeLima
wdelima@kcnsc.doe.gov

J. Hower
jhower@kcnsc.doe.gov

R. L. Mayes
rajnd75@msn.com

[1] Department of Engineering Physics, UW-Madison, Madison, WI, USA

[2] Mechanical Engineering Department, Brigham Young University, Provo, UT, USA

[3] Honeywell Federal, Manufacturing & Technologies, Kansas City, MO, USA

[4] Mayes Consulting, Albuquerque, NM, USA

Introduction

Response reconstruction tests aim to determine whether newly designed parts can survive their intended operational environment. Typically, these tests are performed using a single-axis shaker controlling to one accelerometer on the part of interest in a closed loop [1]. Although this methodology has been standard for many years, there are a few challenges that require solutions. First, each axis is excited individually. This requires extra time and expense to perform the test and increased handling of the hardware which can increase the probability of damage occurring. However, an even more significant concern is that these tests ignore any off-axis motion; while the test may be successfully controlling the accelerometer in the axis of excitation, the part may be subjected to motion in the other directions that is much more severe than the operational environment, leading to spurious failures. Another issue in any kind of shaker testing is that the dynamics of the part change when the shaker is

Published online: 08 April 2023

attached (i.e., there is an impedance mismatch at the interface), and often this causes the part to respond at the lab test resonances at much higher amplitudes than would be observed in the operational environment. This over-testing causes many failures to occur during shaker testing that would not occur during operation, and huge expense can be incurred in needlessly redesigning and retesting the parts.

Engineers have known since the 1970's that the impedance mismatch between the shaker test and the operational environment can cause severe over-testing [2], and although some methods exist for addressing this, they all have significant limitations and none have been universally embraced. Many of the available methods are summarized in Fig. 1.

Six-degree-of-freedom (6DOF) shaker tables using multi–input–multi–output (MIMO) control have been built [3]. These impressive shakers are able to control multiple degrees of freedom in multiple directions simultaneously, addressing some of the issues outlined above with SISO testing. However, the component under test is still required to be bolted to a massive shaker table, so it is typically difficult to match the impedance. Furthermore, the method loses fidelity if the flexible modes of the table are in the frequency range of interest. Perhaps the most high fidelity approach is the Impedance-Matched-Multi-Axis-Testing (IMMAT) methodology [4]. This technique also excites the component in all directions using MIMO control and yet rather than using one massive shaker table, it advocates for using fixturing that mimics the boundary conditions that the part experiences in operation. In the trials to date, this method has recreated dynamic environments far more accurately than single-axis testing [4, 5], yet it presumes that one has enough measurements from the component of interest in the operational environment to determine its modal motion. To perform IMMAT on the component shown in Fig. 1, one would need to have operational measurements on the fixturing as well as the component (though Schultz & Nelson [6] suggest some alternatives in the absence of these operational measurements). If the component was redesigned or otherwise changed after environmental data was recorded, its environment would need to be updated somehow. The increased fidelity of the IMMAT approach comes with increased complexity, introducing new problems. Accelerometer locations and orientations must be decided, shaker voltage limits must be considered as smaller shakers are typically used in these tests, and the list goes on. While Beale et al. [7] investigated methods for accelerometer location selection, and Schultz & Avitabile [8] introduced a shape constrained input estimation method which helped reduce shaker voltage while maintaining similar response accuracy, the increased amount of information required for an IMMAT test still provides a greater barrier to entry than a traditional test.

In order to obtain a compromise between these approaches, in terms of the fidelity and the data that is required, the authors proposed the Transmission Simulator IMMAT approach (TS-IMMAT) [9], in which control is only applied to the fixture or transmission simulator (i.e. the part highlighted red in Fig. 1), and one then relies on a good impedance match between the operation and test environments to achieve an accurate reconstruction of the response on the component of interest. This work presents a derivation that identifies potential sources of error in this method and presents case studies where the method is applied to representative hardware and environment data to understand its advantages and limitations.

In addition to the methods presented above, many other studies have also discussed the limitations of the conventional approach and to present alternatives. For example, Rohe et al. [10] explored the effect of the boundary conditions when testing the BARC structure, designing custom fixtures to optimize the response in a MIMO test, yet they found that this was challenging as a seemingly optimal fixture could have more modes in the test bandwidth while changing the stresses experienced by the part. Jankowski et al. [11] tested the effect of the BARC structure's boundary stiffness on its power spectral density, finding no significant correlation between the two. Taylor explored fixture design in detail, designing tuned mass-dampers to reproduce the

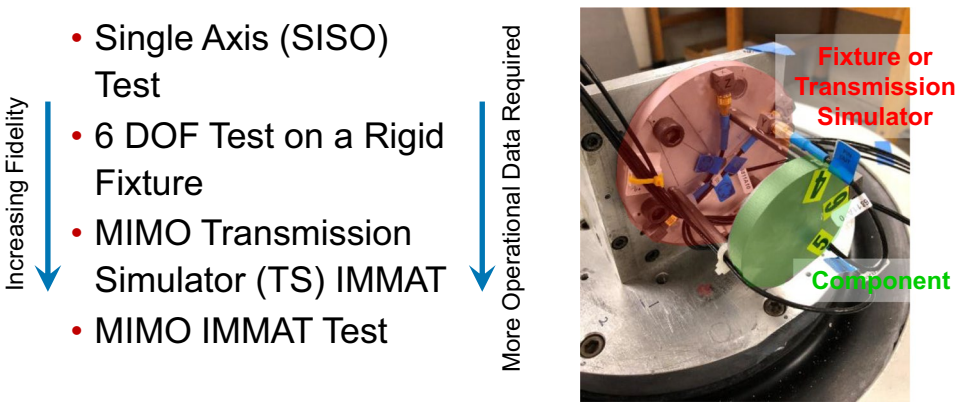

Fig. 1 Various methods have been proposed for dynamic environment testing, each of which has differing fidelity and knowledge of the operational environment

dynamics of the system near the boundary conditions [12]. Reyes & Avitabile [13] explored methods of customizing the forces imparted on a structure in order to better reproduce an environment. Pacini et al. [14] investigated the effect of shaker-structure interactions on the force output of a modal shaker, demonstrating that structural nonlinearities coupled with shaker-structure dynamic interactions caused harmonic distortions in this force output. Dumont et al. [15] discussed various methods of mounting accelerometers as well as their potential to affect a structure's dynamic characteristics.

Before proceeding, it is worth mentioning two other approaches that are frequently used to address the impedance mismatch. When data on the component (green in Fig. 1) is available, one can set response limits, in essence telling the shaker system to reproduce the environment as closely as it can without exceeding those limits. The idea is similar in force limiting [2, 16], although in that case load cells are used between the part and the shaker and the reaction forces are limited. There are some advantages, as the reaction force limits can be estimated using effective mass principles, although several practitioners have found that having load cells connected between the part can be problematic; it introduces additional joints whose preloads are limited by the strength of the force gauges and hence the joints may slip and change the dynamics during the test. (For a comprehensive reference see [17] and see [18] for a case study showing the behavior of industrial joints at typical preloads.) Recently, Van Fossen and Napolitano [19] presented an alternative in which the connection forces are estimated from accelerometer measurements, in essence presenting a hybrid between force and response limiting methods. Any of these methods could prove very effective as long as: 1.) reasonable limits are known and 2.) using those limits does not degrade the accuracy of the environment too much. Alternatively, Larsen, Schultz & Zwink recently proposed an alternative that seeks to replicate the motion at the attachment points of the structure of interest [20] which appears to be promising but requires many shakers if there are more than a small number of connection points.

Returning to the TS-IMMAT approach, prior work has suggested that improving the impedance match of the transmission simulator (TS) will lead to a more accurate reconstruction of the operational environment for the uncontrolled component [21]. Additionally, [21] found that MIMO simulations based on frequency response functions (FRF's) from a modal pretest can do a reasonable job of predicting response reconstruction accuracy for physical MIMO test. To investigate this further, this work presents tests and simulations showing the accuracy with which the response is reconstructed when more of the operational structure is included (i.e. a next-level assembly is used as the TS). Furthermore, to better predict the accuracy of a MIMO test, a condition number threshold is implemented in the simulations to mimic the physical controller that is used in test. This is a continuation of [9, 21, 22].

Theory

Consider the environment reconstruction problem shown in Fig. 2, where we wish to reconstruct the operational response on a subcomponent *S* in the laboratory using a set of shakers. Two possibilities exist: 1.) The response on the subcomponent or on a substantially similar one is measured in the operational environment or 2.) The response is measured near the subcomponent of interest. The former case is depicted in Fig. 2 and the latter is depicted in Fig. 3. The case depicted in Fig. 3 is termed the Transmission Simulator IMMAT method in this work. Both approaches will be discussed in the subsections that follow.

Traditional Environment Reconstruction

When measurements are available on the subcomponent *S*, then a traditional response reconstruction approach can be used. The essence of the process is described below.

The response of a linear system is related to the applied forces through the frequency response function (FRF) (or matrix of frequency response functions) as follows:

$$\mathbf{X}_S(\omega) = \mathbf{H}_{S,i}^{S+TS+V}(\omega) \cdot \mathbf{F}_i(\omega) \tag{1}$$

The subscript of $\mathbf{H}$ denotes that it relates the forcing at input locations i to the response at measurement points S,

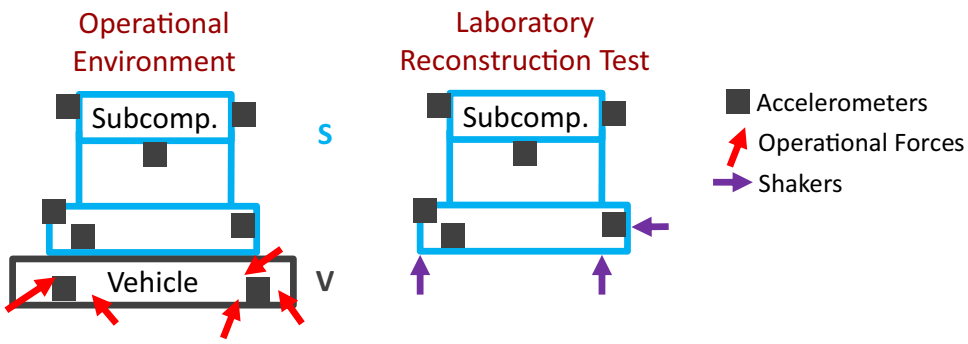

Fig. 2 Schematic of a traditional environment response reconstruction problem in which measurements are taken on a subcomponent of interest (S) when it is connected to a vehicle (V). In the laboratory, we seek to reconstruct the measured operational environment at a set of measurement points using shakers

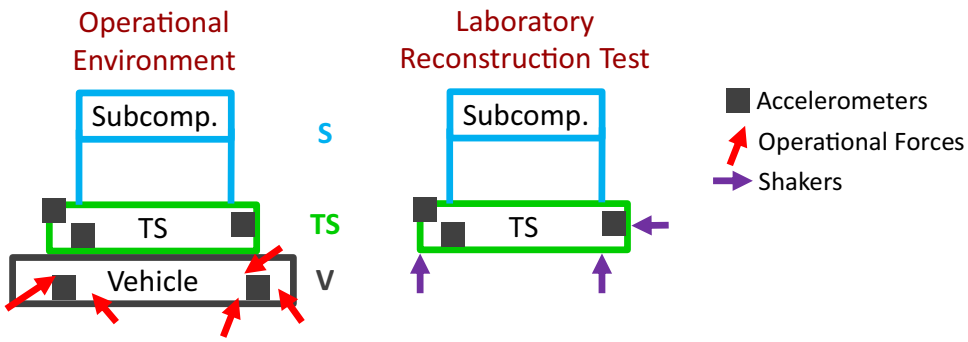

Fig. 3 Schematic of a TS-IMMAT response reconstruction problem in which a subcomponent of interest (S) is connected to a vehicle (V) through a fixture called a Transmission Simulator (TS). In the laboratory, we seek to reconstruct the measured operational environment using shakers

while the superscript indicates that the frequency response is that of the assembly of the subcomponent, *S*, transmission simulator, *TS*, and vehicle, *V*. All FRFs in future equations will be written similarly: i.e., the subscripts will refer to the response and force locations, respectively, while the superscripts will refer to which component dynamics that are included in the FRF. Implicit in this equation is the number of forces and the locations at which they are applied. If the number and location of the forces is adequate then one can invert the FRF matrix to find the forces that the shakers must apply to reconstruct the desired environment $\mathbf{X}_S(\omega)$.

$$\mathbf{F}_i(\omega) = \mathbf{H}_{S,i}^{S+TS+V}(\omega)^{-1}\mathbf{X}_S(\omega) \tag{2}$$

Note that in the end we wish to replicate the power spectrum of the response $\mathbf{S}_{X_S X_S}(\omega) = E\left(\mathbf{X}_S(\omega)\mathbf{X}_S(\omega)^*\right)$, where $E()$ is the expected value, or average over many measurements, but for the derivation below it is sufficient to consider a single realization of the response $\mathbf{X}_S(\omega)$.

In practice, the vehicle is not available for the environment reconstruction test, so the system to be inverted is different (i.e., it consists of the subcomponent, *S*, transmission simulator, *TS,* and shaker dynamics, *Sh*, or $\mathbf{H}_{S,i}^{S+TS+Sh}$) but the desired response can again be obtained so long as the FRF matrix is well conditioned.

$$\mathbf{F}_i(\omega) = \mathbf{H}_{S,i}^{S+TS+Sh}(\omega)^{-1}\mathbf{X}_S(\omega) \tag{3}$$

However, there are several well-known difficulties that can be encountered:

- The force required may exceed the limits of the shaker(s).
- The temporal / frequency characteristics of the field forces on the TS may be difficult to replicate with the lab shakers, i.e., it may be challenging to control the TS input motion to the subcomponent through the desired bandwidth.
- Given N_S shakers, one can only guarantee that the response will be matched at N_S points on the structure $\mathbf{X}_S(\omega)$, but the control can be applied in the least squares sense to produce the closest match that is possible with the given set of shakers.

One can minimize these issues by choosing the shaker locations and add or redesigning the fixturing to change the FRF matrix $\mathbf{H}_{S,i}^{S+TS+Sh}(\omega)$, although the literature contains relatively few guidelines or case studies to help inform these efforts. The present work focuses on an alternative, known as the Transmission Simulator IMMAT method.

Environment Reconstruction with TS-IMMAT

In order to understand the limitations of the TS-IMMAT method, it is helpful to elaborate on the theory that was presented in [21].

In operation, the assembly that consists of a subcomponent of interest, *S*, connected to a vehicle, *V*, through a transmission simulator, *TS*, is excited by forces $\mathbf{F}_V(\omega)$, producing a response on the transmission simulator, $\mathbf{X}_{TS}(\omega)$, which we wish to replicate. The forces are related to the response via a frequency response function $\mathbf{H}_{TS,V}^{S+TS+V}(\omega)$. The subscript denotes that this FRF relates forces on the vehicle, *V*, to response on the transmission simulator, *TS*, and the superscript $S+TS+V$ suggests that the shaker, transmission simulator, and vehicle dynamics are again included in this FRF.

$$\mathbf{X}_{TS}(\omega) = \mathbf{H}_{TS,V}^{S+TS+V}(\omega) \cdot \mathbf{F}_V(\omega) \tag{4}$$

We assume that measurements were only acquired on the transmission simulator, although we will also speak of the response, $\mathbf{X}_S(\omega)$, of the system of interest since these are the responses that we actually want to replicate. A MIMO test is used in which forces, $\boldsymbol{F}_{TS}(\omega)$, are applied to the transmission simulator, with the goal of replicating the measured response.

$$\begin{bmatrix}\mathbf{X}_S^{lab} \\ \mathbf{X}_{TS}^{lab}\end{bmatrix} = \begin{bmatrix}\mathbf{H}_{S,TS}^{S+TS+Sh} \\ \mathbf{H}_{TS,TS}^{S+TS+Sh}\end{bmatrix} \mathbf{F}_{TS}(\omega) \tag{5}$$

$$\begin{bmatrix} \mathbf{X}_{\mathrm{S}}^{true} \\ \mathbf{X}_{\mathrm{TS}}^{true} \end{bmatrix} = \begin{bmatrix} \mathbf{H}_{\mathrm{S,V}}^{S+TS+V} \\ \mathbf{H}_{\mathrm{TS,V}}^{S+TS+V} \end{bmatrix} \mathbf{F}_{\mathbf{V}}(\omega) \tag{6}$$

Using the bottom two rows to equate $\mathbf{X}_{\mathrm{TS}}^{lab} = \mathbf{X}_{\mathrm{TS}}^{true}$, we find the forces that the MIMO controller must apply to match the response on the transmission simulator.

$$\mathbf{F}_{TS}(\omega) = \left(\mathbf{H}_{\mathrm{TS,TS}}^{S+TS+Sh}\right)^{-1} \mathbf{H}_{\mathrm{TS,V}}^{S+TS+V} \mathbf{F}_{V}(\omega) \tag{7}$$

In practice we aren't concerned with this equation because the controller takes care of computing the forces to match the responses on the transmission simulator, but we can use this equation to determine whether it is possible for the controller to achieve an adequate match with the number of shakers and shaker locations that are available. The power spectrum of the TS response, computed using the last two terms in the preceding equation, provides some insight.

$$\mathbf{S}_{X_{TS}X_{TS}}(\omega) = \mathbf{H}_{\mathrm{TS,V}}^{S+TS+V} \mathbf{S}_{F_V F_V}(\omega) \left(\mathbf{H}_{\mathrm{TS,V}}^{S+TS+V}\right)^{*} \tag{8}$$

There could be many forces exerted on the vehicle, so the dimensions of the matrix $\mathbf{S}_{F_V F_V}(\omega)$ could be much larger than those of $\mathbf{S}_{X_{TS}X_{TS}}(\omega)$, exciting many dynamics that cannot be fully observed on the TS. Furthermore, many modes may be active in $\mathbf{H}_{\mathrm{TS,V}}^{S+TS+V}$, adding more complexity to the response $\mathbf{S}_{X_{TS}X_{TS}}(\omega)$. For the transmission simulator method to work, the response $\mathbf{S}_{X_{TS}X_{TS}}(\omega)$ must be spanned by its first N_{TS} mode shapes. If that is the case, and if there are at least N_{TS} sensors so that one can capture those modes, then the power spectrum $\mathbf{S}_{X_{TS}X_{TS}}(\omega)$ can be reproduced. This requires that we apply at least N_{TS} forces to the system. In the studies in this work $N_{TS} = 6$, which means that we can only reproduce the response of six modes at each frequency line. In [21] the authors asserted that the free-free mode shapes of the TS could form an adequate basis for reconstructing the response of the TS, $\mathbf{X}_{\mathrm{TS}}(\omega)$.

$$\mathbf{X}_{\mathrm{TS}}(\omega) = \sum_{r=1}^{N_{TS}} \frac{\boldsymbol{\varphi}_{TS}^{TS} \left(\boldsymbol{\varphi}_{TS}^{TS}\right)^{\mathrm{T}} \cdot \mathbf{F}_{TS}(\omega)}{\left(\omega_r^{TS}\right)^2 - \omega^2 + i\omega 2\zeta_r^{TS}\omega_r^{TS}} + \sum_{r=N_{TS}+1}^{\infty} \frac{\boldsymbol{\varphi}_{TS}^{TS} \left(\boldsymbol{\varphi}_{TS}^{TS}\right)^{\mathrm{T}} \cdot \mathbf{F}_{TS}(\omega)}{\left(\omega_r^{TS}\right)^2 - \omega^2 + i\omega 2\zeta_r^{TS}\omega_r^{TS}} \tag{9}$$

In the above, the first term represents the sum of the N_{TS} modes that we are able to control and the second term is the error, due to all of the modes that cannot be controlled because there aren't enough shakers. There also could be error in the first term due to imperfection in the controller, especially when the controller limits the applied force by truncating singular values, as discussed in Sec. 5. In either case, one can expect that there will be error in the reconstruction on the TS.

$$\mathbf{X}_{\mathrm{TS}}^{lab}(\omega) = \mathbf{X}_{\mathrm{TS}}^{true}(\omega) + \boldsymbol{e}_{TS} \tag{10}$$

Even if the response on the TS was reconstructed perfectly, we still might not reproduce the response perfectly on the subcomponent of interest because the dynamics of the subcomponent can be different in the lab as compared to the field. For example, there may be part-to-part variations between the subcomponent in the field and that present in the true environment. Returning to Eqs. (5)-(6), we see

$$\mathbf{X}_{\mathrm{S}}^{lab} = \mathbf{H}_{\mathrm{S,TS}}^{S+TS+Sh} \mathbf{F}_{TS} = \mathbf{H}_{\mathrm{S,TS}}^{S+TS+Sh} \left(\mathbf{H}_{\mathrm{TS,TS}}^{S+TS+Sh}\right)^{-1} \mathbf{X}_{\mathrm{TS}}^{lab} \tag{11}$$

And substituting in the approximation for $\mathbf{X}_{\mathrm{TS}}^{lab}$, we obtain the following,

$$\mathbf{X}_{\mathrm{S}}^{lab} = \mathbf{H}_{\mathrm{S,TS}}^{S+TS+Sh} \left(\mathbf{H}_{\mathrm{TS,TS}}^{S+TS+Sh}\right)^{-1} \left(\mathbf{X}_{\mathrm{TS}}^{true}(\omega) + \boldsymbol{e}_{TS}\right) \tag{12}$$

which we hope will be a good approximation of the true response, given below.

$$\mathbf{X}_{\mathrm{S}}^{true} = \mathbf{H}_{\mathrm{S,V}}^{S+TS+V} \left(\mathbf{H}_{\mathrm{TS,V}}^{S+TS+V}\right)^{-1} \mathbf{X}_{\mathrm{TS}}^{true}(\omega) \tag{13}$$

This shows that the error in $\mathbf{X}_{\mathrm{S}}^{true}$ can arise from two sources: 1.) Error in reconstructing the response on the TS, due to the term $\boldsymbol{e}_{TS}$ and 2.) Differences in the transmissibility $\mathbf{H}_{\mathrm{S,V}}^{S+TS+V} \left(\mathbf{H}_{\mathrm{TS,V}}^{S+TS+V}\right)^{-1}$ between the assembly on the vehicle and that in the laboratory $\mathbf{H}_{\mathrm{S,TS}}^{S+TS+Sh} \left(\mathbf{H}_{\mathrm{TS,TS}}^{S+TS+Sh}\right)^{-1}$. Note that the first source of error depends strongly on the number of shakers that are available; if there are not enough shakers available to fully control the TS then it may be impossible to make the term $\boldsymbol{e}_{TS}$ sufficiently small.

In our prior work [21], and again in the results that will be presented here, we have found that these two sources of error are important. Specifically, the results showed that even when the response of the TS was reconstructed quite well, the response of the system of interest still had significant errors. To better understand this observation, Sec. 3 will present a simple case study that illustrates the problems that can be encountered with this method.

Reconstruction Error Metrics

In the results that follow, two error metrics were used to quantify the difference between the target environment and that achieved in the laboratory. The average dB difference of two ASDs for all relevant accelerometer channels at a frequency line is defined as follows.

$$e_{ASD}(f_i) = \sqrt{\frac{1}{n_{accels}} \sum_{k=1}^{n_{accels}} \left[dB[\boldsymbol{S}_{X_kX_k}(f_i)] - dB[\boldsymbol{S}_{X_kX_k,lab}(f_i)] \right]^2} \tag{14}$$

For this work, $\boldsymbol{S}_{X_kX_k,lab}$ is the simulated or experimental acceleration ASD for the kth accelerometer DOF and $\boldsymbol{S}_{X_kX_k}$ is the operational ASD for the same DOF. After computing an error value for each frequency line, a final metric is computed using Eq. (15).

$$e_{ASD} = \sqrt{\frac{1}{n_{freq}} \sum_{i=1}^{n_{freq}} e_{ASD}(f_i)^2} \tag{15}$$

This final error number represents the average dB error across all accelerometers and frequency line. A low error metric communicates a successful reconstruction test and will be used moving forward to compare various tests.

This error metric was used to create a shaker placement algorithm, which is detailed in the Appendix. That was used to select optimal shaker locations for various tests that were performed in the precursor to this work [21]. While that method was found to be effective, over various tests it was found that the results were not very sensitive to the shaker locations so long as an acceptable set was found; in other words, there were many possible sets of shaker locations that gave similar results. Hence, to simplify the presentation in this work, a single set of shaker locations was used that was selected based on experience and engineering judgement.

Mass-Spring System Case Study

A mass-spring model was created to mimic the dynamics that are experienced in practice, while keeping the system as simple as possible, and is shown in Fig. 4. The subcomponent of interest is mass 1 and it is connected to the transmission simulator, masses 2 through 5, which are connected by relatively stiff springs so that the TS has relatively few modes that are active at lower frequencies. Four masses were selected for the TS so that it would have two modes that mimic its rigid body behavior as well as two elastic modes to exercise the TS-IMMAT method. The vehicle is comprised of masses 6 through 9, and their connecting springs are chosen to be about twenty times less stiff, to approximate a realistic case in which the vehicle has many modes in the frequency range of interest. The parameters used were: $m_1 = 0.5$, $m_2 = 1.1$, $m_3 = 1.15$, $m_4 = 1.08$, $m_5 = 1.03$, $m_6 = 1.2$, $m_7 = 1.3$, $m_8 = 1.22$, $m_9 = 1.28$ kg, and for the subcomponent $k_{13} = 5.2$, $k_{14} = 5.2$, transmission simulator $k_{23} = 20$, $k_{34} = 20$, $k_{45} = 20$, $k_{26} = 20$, $k_{59} = 20$, and vehicle $k_{67} = 1.1$, $k_{78} = 0.95$, $k_{89} = 1.02$, $k_6 = 0.8$, $k_9 = 0.84$ N/m. These parameters do not necessarily represent the mass and stiffness of the system studied later. They are merely meant to represent a case study where the transmission simulator is much stiffer than the vehicle, as is the case in the next section.

Table 1 Descriptions of the two case studies with DOF referenced from Fig. 5

Label	Control DOF	Forcing Input DOF
Case Study 1	3, 4	3, 4
Case Study 2	2, 5	3, 4

The response in the operational environment was created by applying a force with unit magnitude at each frequency line to DOF 6 and DOF 9 as illustrated in Fig. 4. This is the response that we wish to reconstruct. Then, a new assembly was created consisting only of the TS and subcomponent, as is the case for our experimental work.

Two case studies will be considered, summarized in Table 1. In each case study, an attempt was made to

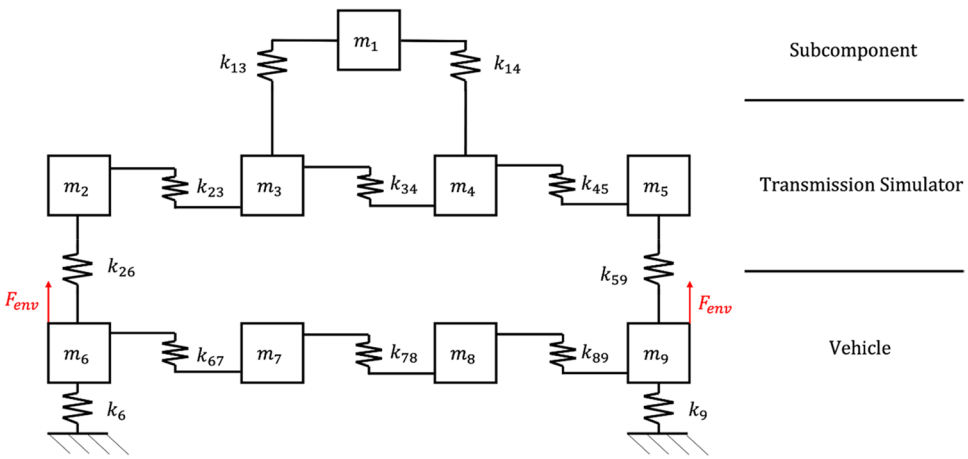

Fig. 4 Mass-spring system representing a vehicle (V), transmission simulator (TS), and subcomponent (S). This corresponds to the actual operating configuration of the system

reconstruct the environment response using only the assembly consisting of the TS and subcomponent.

Figure 6 shows the response of all DOF on the TS and subcomponent for Case Study 1. In this figure, "Lab" represents the attempted reconstruction using the system in Fig. 5 and "Environment" represents the response of the full assembly in Fig. 4. As expected with two forcing inputs controlling to two DOF, the interface DOF (3 and 4) are reconstructed perfectly. Because the subcomponent (DOF 1) is connected only to these two DOF, we obtain near perfect reconstruction of the response on the subcomponent (DOF 1). Interestingly, the response of DOF 2 and 5 is accurate below 1.5 rad/s but becomes highly inaccurate above that frequency.

The errors in DOF 2 and 5 above 1.5 rad/s can be explained if one considers the modes of the system. The assemblies have the natural frequencies shown in Table 2. In the full assembly, the motion of the TS is well approximated with two modes: 1.) rigid body bounce and 2.) asymmetric rotation (which has the appearance of a rigid body rotation mode but involves flexure of the springs because the masses are not free to rotate). Using Eq. (9), the transmission simulator response can be reconstructed as a linear combination of its modes. Because two forcing inputs are used in the case study, $N_{TS} = 2$, so the first two modes of the transmission simulator should be perfectly reconstructed. Therefore, the full, physical response of the transmission simulator DOF (2 through 5) should

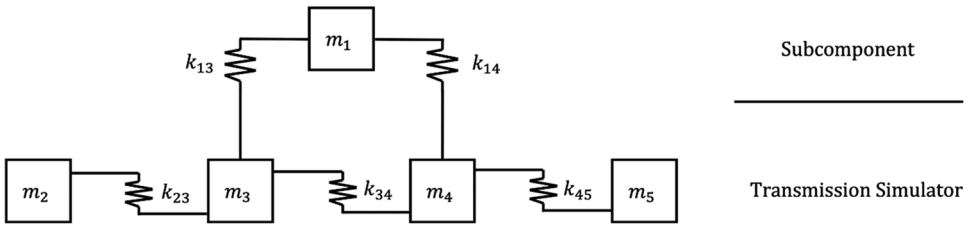

Fig. 5 Mass spring system representative of an experimental setup that only includes a TS and subcomponent. This corresponds to the configuration tested in the laboratory

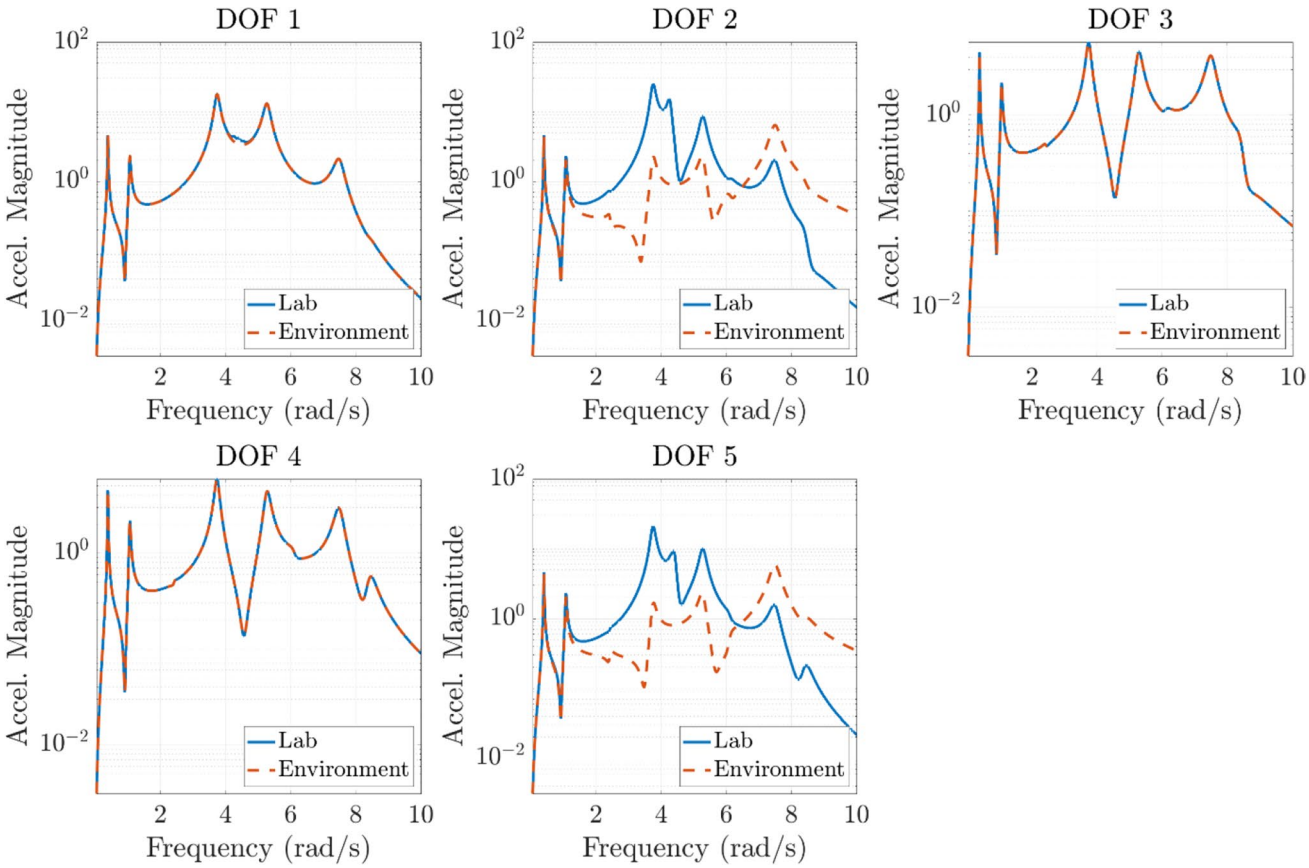

Fig. 6 Response of subcomponent and TS for Case Study 1

Table 2 Natural frequencies (rad/s) of the assemblies in Figs. 4 and 5

Assembly / Nat. Freq	S + TS + V (Fig. 4)		S + TS (Fig. 5)	
ω_1	0.39	Rigid Bounce on k_6 and k_9	0.00	Rigid Body
ω_2	1.07	Veh. 1st Bending + TS Bounce	3.41	TS Assym
ω_3	1.49	Veh. 2nd Bending	4.51	TS 1st Bending
ω_4	2.42	Veh. 1st Bending + TS Rot	6.46	Coupled
ω_5	3.75	TS 1st Bending	8.11	TS 2nd Bending
ω_6	5.28	Subcomponent Bounce	n/a	

be accurate in the frequency range where these first two modes are dominant in the environment response. In contrast, the modal forces for the uncontrolled modes may be completely different from the environment, depending on the location where the control forces are applied.

In Fig. 7, the black boxes represent the initial positions of each mass and the red boxes show the relative displacements of each mass when the system moves in the mode of interest. At 3.75 Hz, the TS experiences its first bending mode, as shown in Fig. 7a. At this frequency, this motion causes the response at DOF 2 and 5 to deviate even if DOF 3 and 4 match the desired environment perfectly. In other words, the error term $\boldsymbol{e}_{TS}$ in Eq. (10) becomes large. Looking again at the responses in Fig. 6, the motion corresponding to this mode seems to have a shoulder that extends below 2 rad/s, and hence this mode seems to be responsible for the loss of accuracy that was observed above 1.5 rad/s. Note that this same TS bending mode exists for the S + TS assembly (in Fig. 5) but there it occurs at 4.5 Hz, as shown in Fig. 7b and listed in Tab. 2.

In Case Study 2, DOF 2 and 5 are controlled with forcing inputs at DOF 3 and 4. This case is representative of the tests presented in the next section where the control DOF are not precisely at the interface and the forcing inputs do not completely control the locations where the transmission simulator connects to the next level assembly. The results from this case study are presented in Fig. 8, and show that, while the two shakers are able to reconstruct the response perfectly at DOF 2 and 5, once again the response at the other two DOF (DOF 3 and 4 in this case) is highly inaccurate above 1.5 rad/s. Furthermore, because those DOF connect to DOF 1, the response of DOF 1 also loses accuracy above 1.5 rad/s.

Experimental Case Study

To further evaluate the TS-IMMAT methodology, it was tested on the system shown in Fig. 9. The photo shows the most complicated subsystem considered. The actual flight configuration consisted of the assembly shown with data acquisition systems bolted onto the bulkhead plate, and the whole assembly was bolted to a fiberglass tube and into the sounding rocket. In a previous work [21] reconstruction tests were performed using assemblies with the same plate (TS) and stool (subcomponent); however, these assemblies did not include the pillars or the bottom bulkhead. The accelerometers are positioned in a cylindrical coordinate system, and the directions referenced throughout the rest of this analysis are specified in Fig. 9.

This assembly flew inside a sounding rocket flown for Kansas City National Security Campus in July 2019. The assembly was instrumented with three triaxial accelerometers on the plate and three triaxial accelerometers on the stool. During flight, the rocket experienced four main phases: boost, coast, deployment of the drogue parachute, and deployment of the main parachute. The operational

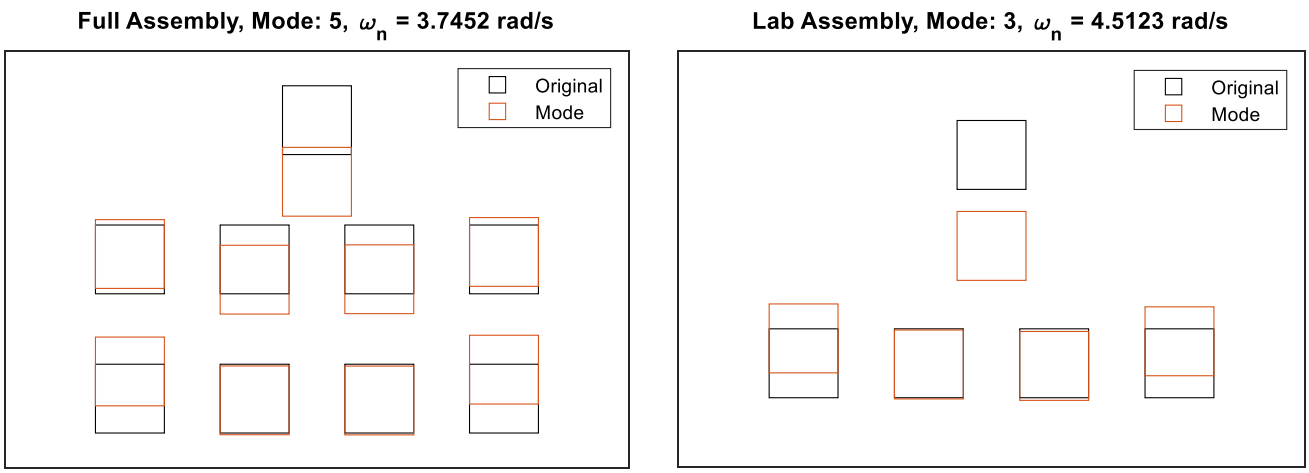

Fig. 7 Mode Shapes of the (**a**) S + TS + V system and (**b**) S + TS system

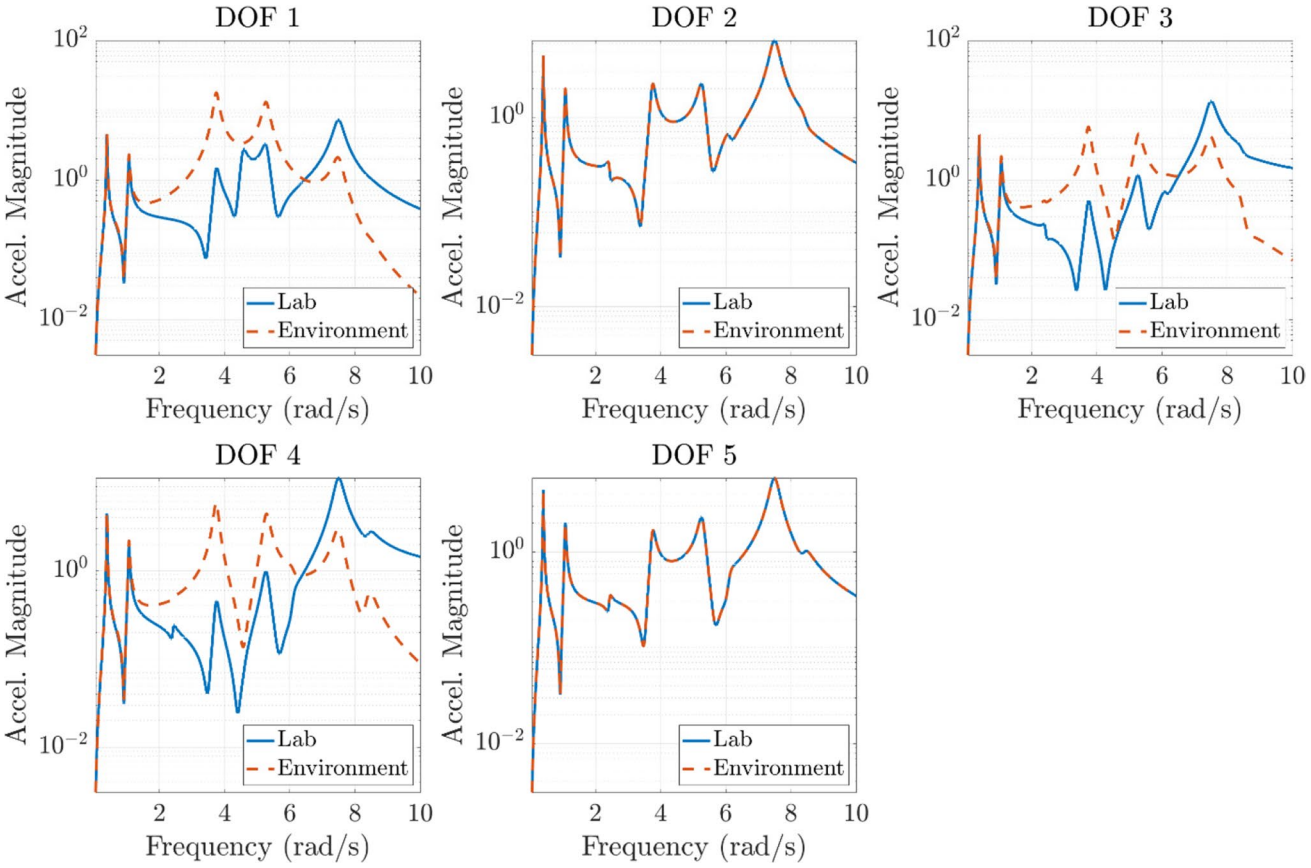

Fig. 8 Response of subcomponent and TS for Case Study 2

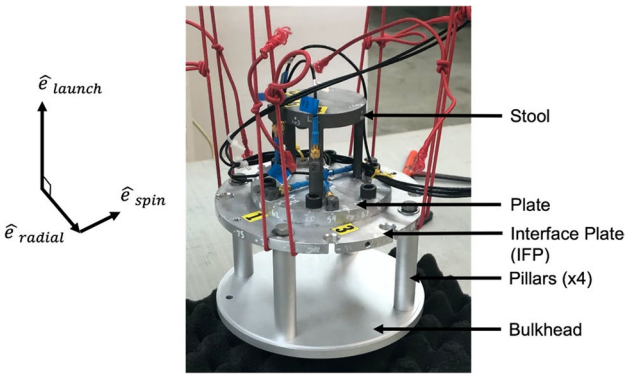

Fig. 9 The instrumented next-level assembly

environment power spectral density (PSD) profiles were constructed from acceleration time data from 0.5 to 20 s after launch. This time frame captures the boost and coast phase while excluding any shock event at ignition along with the deployment of the parachutes.

The frequency spacing of the PSD profiles generated was 5 Hz, and the testing bandwidth of interest was 100 to 4000 Hz. Unfortunately, the data from the first accelerometer in the radial direction (channel 1) only recorded noise during flight. Thus, there are eight channels on the plate and nine channels on the stool that recorded useful data.

Three assemblies will be considered in the following analysis, and the test setups for each assembly are shown in Fig. 10. For each configuration, the goal is to reconstruct the environment on the plate using six small shakers using MIMO control. To assess the success of a TS-IMMAT test for each configuration, the accuracy of response on the controlled plate and on the uncontrolled stool will be compared. Our prior work [21] presented TS-IMMAT reconstruction tests on Configurations A and B; this work will focus on comparing those with Configuration C. Furthermore, the results will be evaluated in light of the theory presented in Sec. 2.

Roving Hammer FRF's

To be able to simulate a MIMO test, the frequency response functions, e.g., in Eq. (8), are needed. These were obtained by performing a modal roving hammer test on each configuration. For each configuration, the structure was excited at various locations and the response was measured. Data

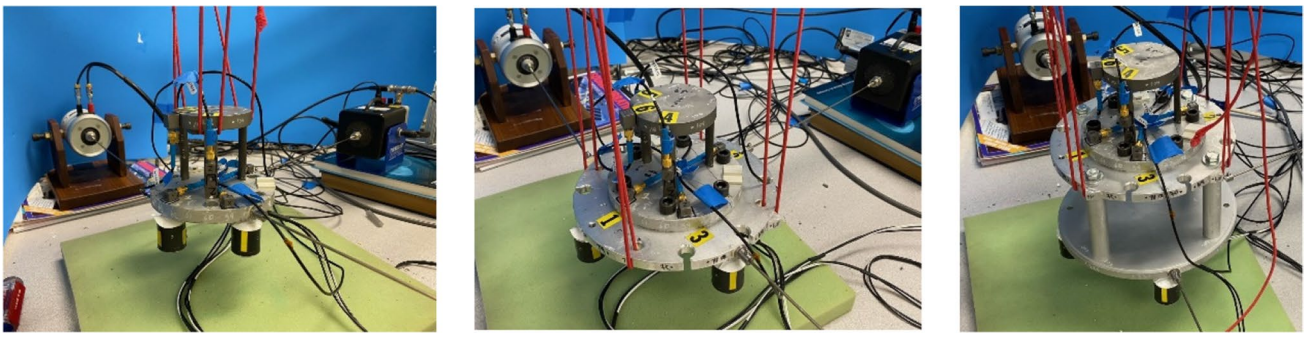

Fig. 10 The three assemblies tested are Configuration A with the stool and plate, Configuration B with the stool, plate, and IFP, and Configuration C with the stool, plate, IFP, pillars, and bulkhead

Physics Abacus hardware and SignalCalc 730 software recorded the FRF's in the bandwidth of 0 to 4000 Hz with a frequency resolution of 5 Hz to match the environmental acceleration profiles. While these FRF's could be used to select an optimal set of shaker locations, we used the locations shown in Fig. 10 to maintain consistency between setups. Thus, the MIMO tests were simulated using the portions of the FRF corresponding to the chosen shaker locations, and these results are shown later to demonstrate the accuracy of the simulations. It's worth noting that this FRF does not account for the dynamics of the shakers that are attached to the device under test. Thus, the roving hammer FRF is an approximation of the MIMO test FRF, and some error is expected in the simulation predictions. Though not implemented here, shaker dynamics can be included in test simulations via dynamic substructuring, as Mayes [23] and Schultz [24] have shown.

Experimental Methodology

The workflow for performing a TS-IMMAT reconstruction test is as follows. The measured FRFs are used to simulate the MIMO test using Eq. (8). To compare test results between different configurations more accurately, similar sets of shaker locations were used on each configuration. The simulated test results are discussed later, to give an idea of how accurate these simulations are.

Then, to perform the actual MIMO test, shakers were attached at the desired locations. Three SIEMENS Q-MSH electromagnetic (EM) inertial shakers were used to excite the assembly in the launch direction. These three shakers were attached directly to the structure using super glue. In the off-launch directions, two Modal Shop EM shakers and one LDS EM shaker were connected to the assembly via stingers made of piano wire which were also attached with super glue. For each configuration, the Modal Shop shakers excited the structure radially, and the LDS shakers were attached to an angle block to excite torsion in the structure. In Configuration A, the shakers were attached to the plate. In Configuration B, the shakers were attached to the interface plate, and in Configuration C, all shakers were attached to the bottom bulkhead.

To perform the MIMO test, Data Physics Abacus hardware and Data Physics SignalStar Matrix controller software were used. Per requirements of the TS-IMMAT approach, the closed-loop MIMO software only controlled to the accelerometers on the plate. Because one accelerometer channel recorded noisy data during flight and another channel started to record poor measurements in the laboratory, only seven accelerometer channels were controlled to. The control profiles were the PSD matrices constructed from the flight data as described earlier. The remaining 9 accelerometer channels on the stool were not controlled to, but they were measured.

MIMO Test Results

Figure 11 presents the auto-spectral densities (ASD's) for the accelerometer channels on the controlled plate. The black line is the operational environment profile that is being controlled to, and the cyan line is the response recorded during the reconstruction test. Additionally, for each channel, the dB error computed using Eq. (15) is provided in each subplot's title.

The reconstruction on the plate was fairly accurate throughout the testing bandwidth, having an error of only 7.2 dB. While we presume that one would not have measurements on the component of interest in practice, we had accelerometers on the stool so we could evaluate the performance of the proposed TS-IMMAT approach. Figure 12 illustrates the measured ASD's of the accelerometer channels on the stool (cyan) with the environment profiles generated from the flight data (black).

Unsurprisingly, the error in reconstructing the stool response is higher than the error in the reconstructing the plate response. Up to 500 Hz, the error is relatively low, but it increases significantly at higher frequencies, presumably

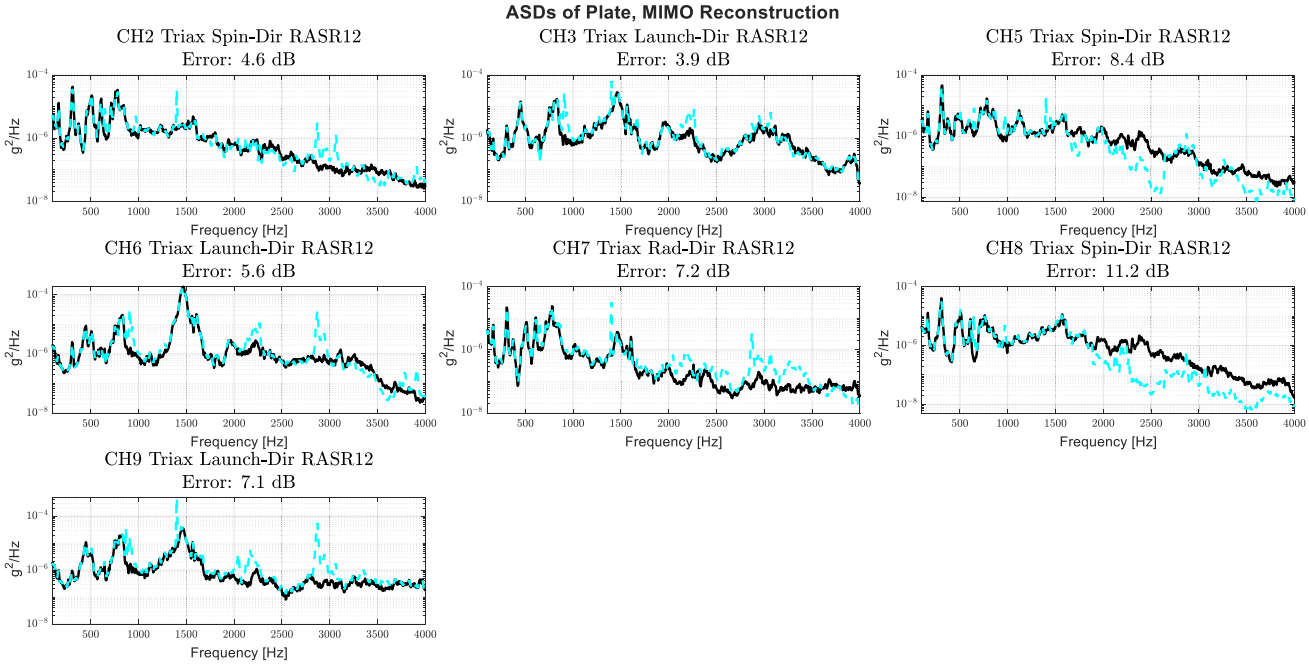

Fig. 11 Reconstruction ASDs of the controlled accelerometers on the plate (cyan) along with the control ASDs (black) for Configuration C

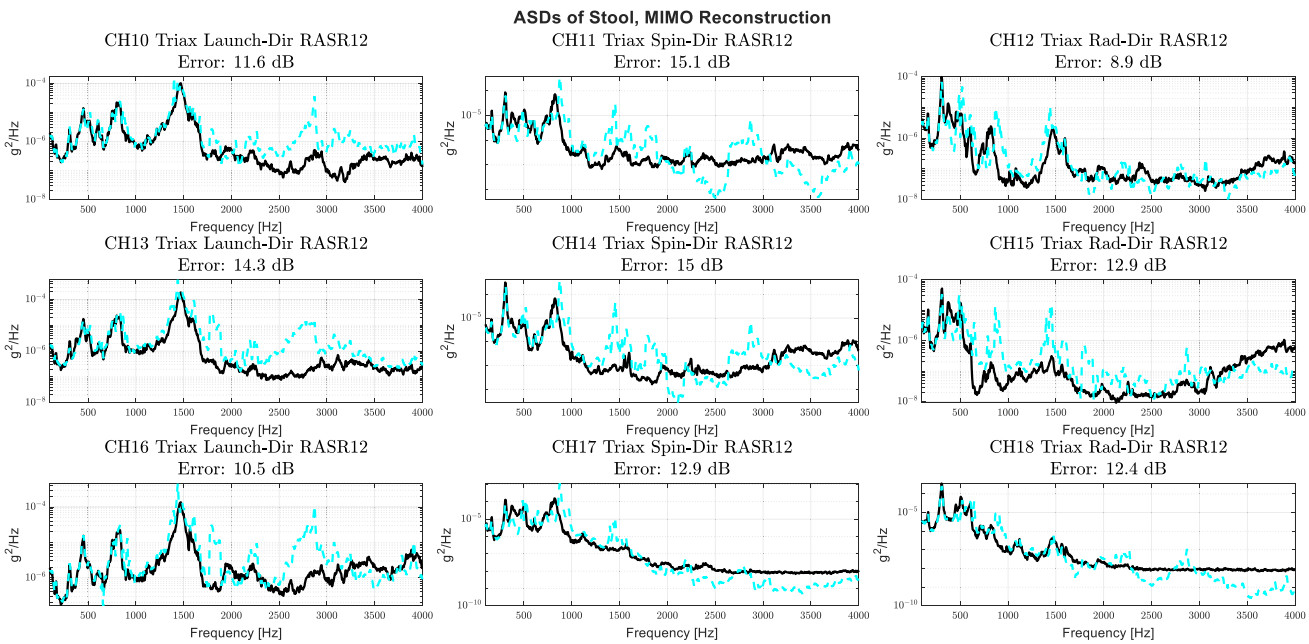

Fig. 12 Measured ASDs of the uncontrolled accelerometers on the stool (cyan) along with the environment ASDs (black) for Configuration C

due to a larger number of active elastic modes. Thus, the total error in the bandwidth is a higher 12.8 dB. It is interesting to compare these results to those obtained on Configurations A and B. Table 3 compares the error metric obtained in each of these configurations from 100 to 2000 Hz and 100 to 4000 Hz. Each of these tests was performed with a condition number threshold of 0.01 to reduce the voltage levels required for each shaker. An in depth discussion of the condition number threshold is given later in this paper. It is worth noting that all configurations give very similar results in the 100–2000 Hz frequency band, and there are only a few differences for the 100–4000 Hz range.

Table 3 Error in experimental reconstruction for three assemblies tested

Assembly	Error from 100–2000 Hz (dB)		Error from 100-4000 Hz (dB)	
	Plate	*Stool*	*Plate*	*Stool*
Configuration A	2.5	10.1	3.1	11.2
Configuration B	2.0	11.2	2.9	14.3
Configuration C	3.4	11.3	7.2	12.8

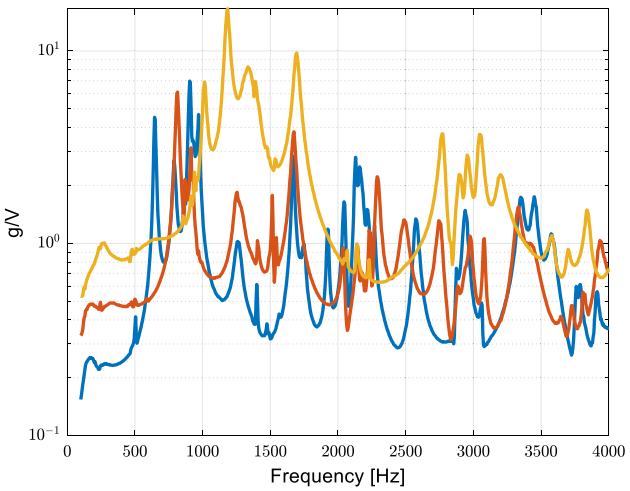

Fig. 13 Composite of the Frequency Response Functions measured on each of the configurations: (yellow) Configuration A, (red) Configuration B, (blue) Configuration C

Discussion

First consider the controllability of each assembly. The control was applied only to the plate accelerometers, and the controller was able to match their responses very accurately in all cases except for Configuration C at higher frequencies. The composite frequency response of each configuration is shown in Fig. 13, which shows that Configurations A and B have far fewer active modes than Configuration C, explaining this differerence. However, the far more flexible transmission simulator in Configuration C only significantly affects the results above 2000 Hz.

The previous testing of Configuration A and Configuration B suggested that using more of the original operational structure would improve the response accuracy for the controlled transmission simulator (plate) and for the uncontrolled subcomponent (stool). Those results had been obtained using different sets of shaker locations on the two configurations and potentially different settings in the control that limited the effectiveness of the shakers. When these issues were corrected, it is possible to obtain very good control on the plate for all configurations as seen here. In the results above, the accuracy on the stool was similar for all configurations. This suggests that none of these configurations improves the transmissibility of the plate's response to the stool enough to overcome the errors in reconstructing the plate (or TS) response. Hence the error term $\boldsymbol{e}_{TS}$ in Eq. (12) seems to be much more significant than error due to noise or limitations of the controller The errors at the control accelerometers are quite low, as shown in Fig. 11. This might suggest that $\boldsymbol{e}_{TS}$ is also low, but that is only true if enough control accelerometers are available to ensure that all active modes in the TS are accurately captured. This does not seem to be the case. In Fig. 12 the response on the stool only tracks the desired environment to 500 Hz or so, so beyond that point we expect that the modes of the TS are active enough to introduce significant errors in the stool.

Only six shakers are available, so at most six modes can be controlled at each frequency line. As shown in Fig. 13, the assembly has many more modes as more of the next assembly is added. However, the modes considered in Fig. 13 are those of the entire assembly. If one considers only the transmission simulator, then a simple finite element model that was constructed as part of this work places the first flexible mode for Configurations A and B at around 3300 Hz and 2700 Hz respectively. For Configuration C, the pillars and bottom bulkhead are quite flexible which drops the first flexible mode of the TS down to 900 Hz. Therefore, Configuration C is not controllable for a much larger portion of the total bandwidth compared to the other two configurations. This, perhaps, explains the large error term in Eq. (9) for Configuration C relative to the lower errors observed for Configurations A and B.

Another important factor to consider in deciding how much of a part's attached structure should be included in a test is the capabilities of the shakers. Since IMMAT tests use smaller shakers that have lower voltage limits, it is common for these limits to be exceeded, preventing a test from running. As mentioned previously, a condition number threshold of 0.01 was used for the previous tests because some of the shakers' voltage limits would have been exceeded in testing configuration C without the threshold. As seen in Table 4, the required shaker voltage increases when more of the attached structure is included in a test. This is not surprising given that including more of the assembly makes the structure heavier, requiring greater shaker force.

It is worth discussing the effect of shaker locations on the reconstruction error. The shakers were placed at the locations used in these tests to avoid some common problems in IMMAT tests. One is when two shakers are placed opposing each other, resulting in higher required shaker voltage and poorer reconstruction. The locations previously used largely

Table 4 Average Shaker RMS Voltage in Tests Performed on Each Configuration

Assembly	Average Shaker RMS Voltage (V)	
	100–2000 Hz	100–4000 Hz
Configuration A	0.072	0.083
Configuration B	0.105	0.156
Configuration C	0.236	0.281

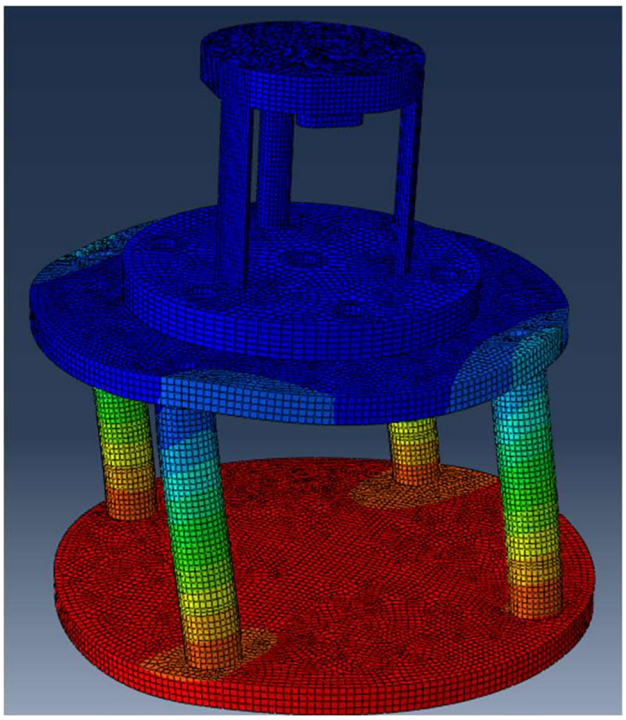

Fig. 14. 2nd Fixed Plate Mode of Configuration C, 451 Hz

avoided this problem as no shakers directly opposed any others. Another problem is failing to excite the device under test in any of the rigid body degrees of freedom, and the set of shaker locations we used avoids this problem as well, exciting in the radial, spin, and launch directions.

One area of uncertainty, though, was where to place the shakers on configuration C. As shown in Fig. 10, we attached the shakers to the bottom bulkhead plate in the previous tests, assuming that this would most accurately match the in-flight load path and yield the most accurate reconstruction. It is possible that there are modes excited in the test, such as the second fixed-plate mode shown in Fig. 14, wherein the bottom bulkhead plate and columns deform significantly while the stool does not, though. This mode was obtained by fixing the nodes at the locations of the accelerometers on the plate in a simple FEM of configuration C, and it should represent how the structure deforms when plate accelerometers are controlled to in a

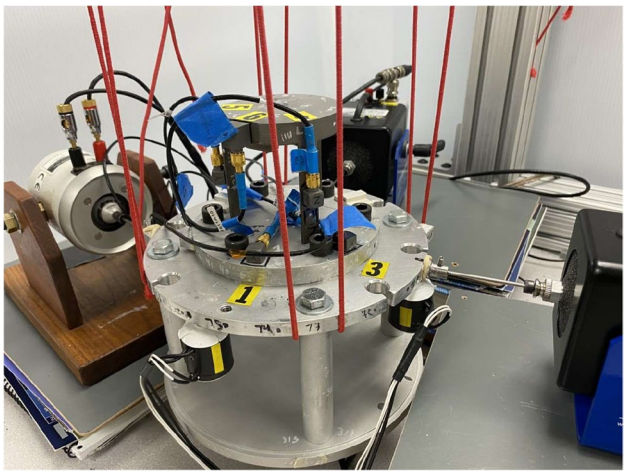

Fig. 15 Test Setup on Configuration C with Shakers Attached to Interface Plate

Table 5 RMS dB Error on Configuration C when Shakers are attached to Bulkhead Plate and Interface Plate

Shaker Locations	Error from 100–2000 Hz (dB)		Error from 100-4000 Hz (dB)	
	Plate	*Stool*	*Plate*	*Stool*
Bulkhead Plate	3.4	11.3	7.2	12.8
Interface Plate	4.8	13.0	7.9	14.2

test. It seems possible, therefore, that the stool response would be more accurately reconstructed by attaching the shakers to the interface plate instead, as by doing so, the shakers would not have to control these fixed plate modes.

To test this theory, a physical test was performed with the shakers attached to the interface plate on configuration C as shown in Fig. 15. The shakers were placed roughly at the same locations as the previous test on configuration B. Shorter stingers were used in this test, but we have found that our shakers can control the axial stinger modes well, so stinger length should not affect the reconstruction error in this case. All other test settings were kept the same, and a condition number threshold of 0.01 was implemented on the FRF matrix.

The results in Table 5 show that similar dB errors were obtained whether the control was on the bulkhead plate or interface plate. In this comparison the impedance of both configuration is nearly the same, differing only due to the added mass and stiffness that the shakers add. Hence, the primary difference is potentially in the controllability, although both setups have the same number of shakers in the same orientations. Considering that the reconstruction accuracy remains about the same for both sets of shaker locations, it seems that neither improves the controllability

of the system dramatically, although one might expect that having the shakers closer to the control accelerometers would improve controllability. It doesn't seem that reconstruction accuracy is very sensitive to changes in shaker locations, provided that the shakers are placed to minimize interactions between them and to excite the structure in all rigid body degrees of freedom.

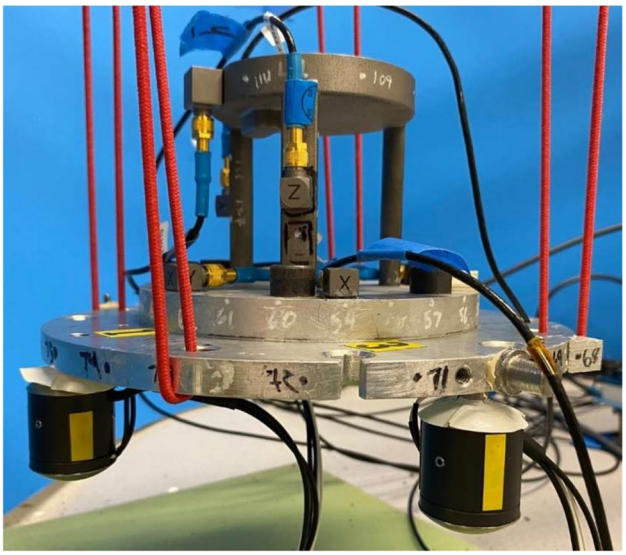

Fig. 16 Photo of test setup for Configuration B-2 with three shakers in the launch direction and all others removed

Configuration B2 – Test with Small Error Term in Eq. (9)

This hypothesis was further tested by repeating the test on Configuration B while using only three shakers to seek to control all of the modes in the launch direction, as shown in Fig. 16. In this direction the first mode of the transmission simulator occurs above 2500 Hz, and the first mode of the assembly in the launch direction is also above 2500 Hz. Hence, according to the theory presented earlier, one would expect to be able to achieve excellent control of the transmission simulator in the launch direction, and that the system of interest (the stool) should also achieve the desired response.

The results, presented in Fig. 17, confirm this hypothesis. Up to 500 Hz, the errors in the launch direction are 0.8 and 2.7 dB RMS on the plate and stool respectively. Thus, the three Q-source shakers reproduce the environment on the plate and stool very accurately at low frequencies. At higher frequencies, the plate response is reconstructed well, but there is significant error near 600 Hz in the stool response, which in the vicinity of the first bending mode of the assembly. The results slowly degrade above this frequency, and by 2000 Hz, the error grows noticeably as we approach the first axial mode of the plate. The three available shakers are insufficient to control the four modes (three rigid body and one elastic) that are active at this frequency. While there is error at higher frequencies, the reconstruction is quite accurate at low frequencies where rigid body motion dominates, demonstrating that the transmission simulator theory holds true.

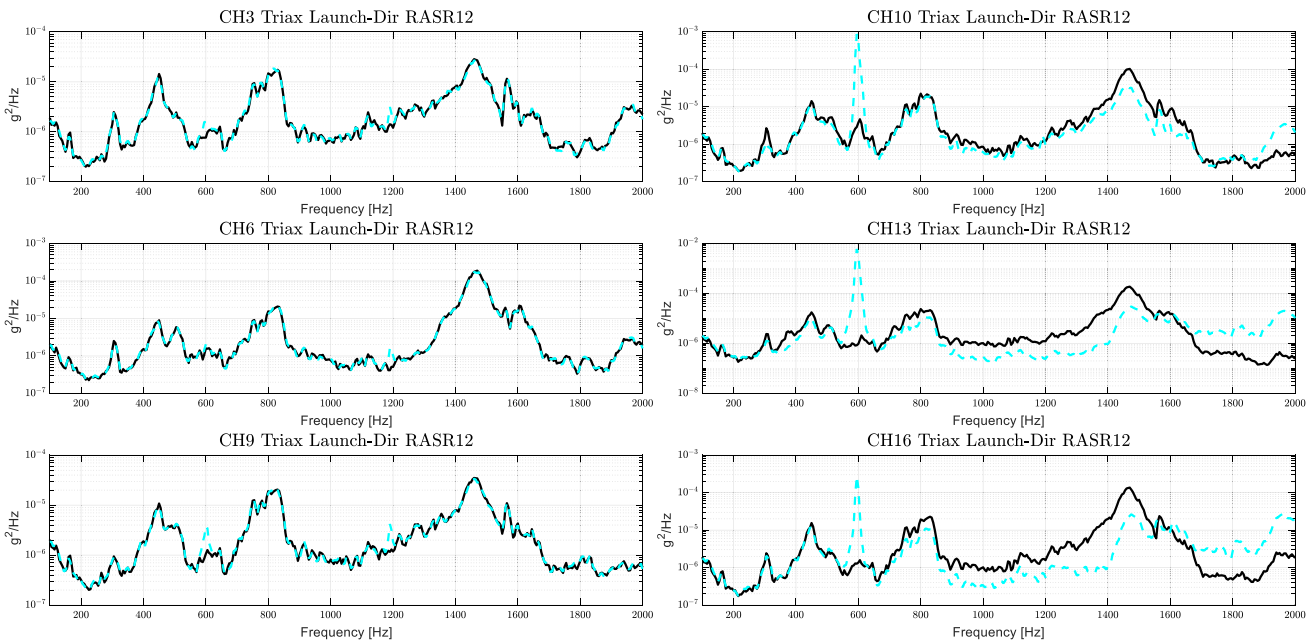

Fig. 17 Response of the stool on plate system in the launch direction, with Plate accelerometers (CH3, CH6 and CH9) and Stool accelerometers (CH10, CH13 and CH16)

Configuration A-2 – Test with Small Transmissibility Mismatch in Eqs. (12) and (13)

As mentioned earlier, the second source of error in a TS-IMMAT test is the mismatch in transmissibility (or impedance mismatch) between the lab and true environment. To test the importance of this transmissibility term in Eqs. (12) and (13), a simple experimental study from [11] is revisited. Configuration A from Fig. 10 was suspended in the laboratory using a bungee cord suspension system. The plate was then struck randomly for 10 s, and time histories from the accelerometers were recorded during these 10 s of excitation. These time histories were then used to construct ASDs and CSDs that served as the new operational environment profile. Controlling to this new environment profile, a MIMO test of the same system under the same free-free boundary conditions was performed. Because the system (subcomponent plus TS) exactly matches that which will be used during MIMO control, except for any change in the impedance due to attaching the shakers, the transmissibility should be nearly identical in Eqs. (12) and (13). In contrast, the error term due to controlling up to 12 modes with 6 shakers, could remain as large as it was in the other case studies. A set of shaker locations was chosen to minimize plate response error for the new test profile, and a MIMO test controlling to 7 accelerometers on the plate was then performed, i.e. the TS-IMMAT method because the stool accelerometers were not included in the control. Rather than showing all of the individual spectra, Fig. 18 presents the average of the measured ASDs (i.e. the trace of the CSD matrix) of the controlled accelerometers on the transmission simulator (left) and the sum of the measured ASDs of the uncontrolled accelerometers on the subcomponent (right).

The results from Configuration A-2 show excellent agreement between the desired environment and the reconstruction. Using the metric provided in Sec. 2.3, the error from 100 to 5000 Hz on the plate and the stool is 5.9 dB and 8.3 dB respectively. The errors are dominated by several single-frequency-line deviations at high frequencies, but these are attributed to noise in the data acquisition and control systems, because this environment was at a much lower amplitude and hence near the noise floor of the systems. Nevertheless, if this is ignored then the results are outstanding in this case study on both the transmission simulator and the object of interest. This suggests that the transmissibility, which is influenced by the boundary conditions in test, is extremely important. Unfortunately, in most cases of interest one does not have the entire vehicle to test and so the impedance is not likely to match as well as it does in this case study.

Simulations with Condition Number Threshold

The case studies have highlighted how challenging environment reconstruction can be, with the results being sensitive to the boundary conditions, shaker locations, etc.… While there are still no simple metrics that can predict the success of a MIMO test, one can readily simulate a MIMO test using the equations presented in Sec. 2.2 and frequency response functions measured in a roving hammer test. This was done in a precursor to this work to find

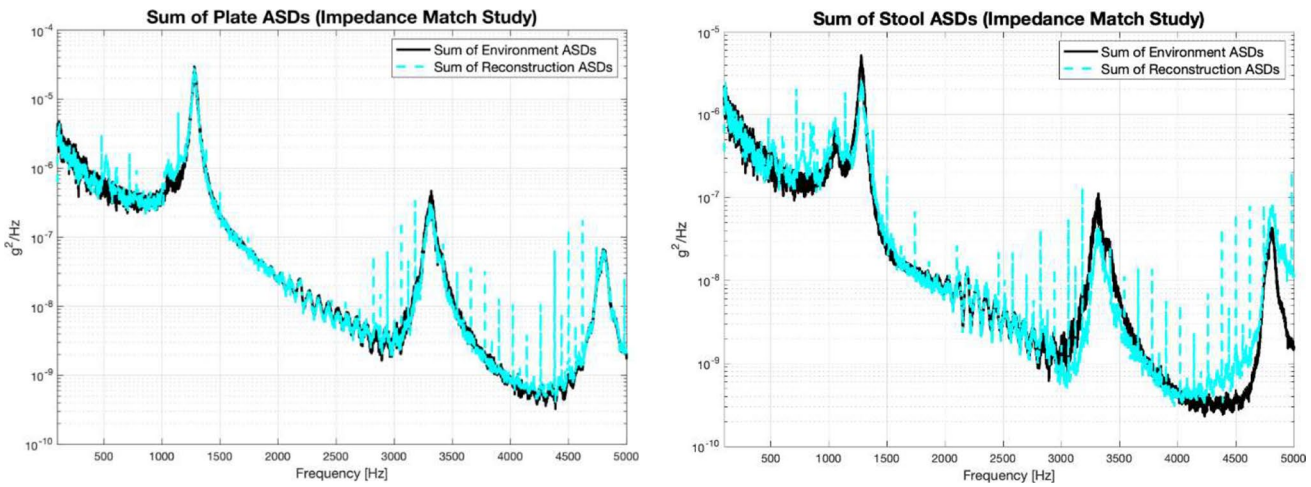

Fig. 18 Measured ASDs of the plate (left) and the stool (right) from Configuration A-2, the case study where there is a near perfect impedance match between lab and the true environment

optimal shaker locations [21]. However, those simulations in initially predicted errors in the control accelerometers that were much lower than what was actually observed in experiment. The Data Physics control software used in this work is known to implement a condition number threshold when inverting the frequency response function matrix to limit the forces that must be exerted by the shakers. Thus, this section will explore how to implement a condition number in simulation and compare simulated results with and without a condition number threshold.

Condition Number Threshold Implementation

A condition number threshold is traditionally used when inverting ill-conditioned matrices to limit the magnitude of elements in the inverse. In the MIMO simulation theory, an inversion only takes place in Eq. (3) when solving for the forces and hence $\boldsymbol{S}_{FF,est}(\omega)$. In the simulations used in this work, the following procedure is used to compute the pseudoinverse of the desired FRF, which is denoted $\boldsymbol{H}_{XF}(\omega)$ in the following, in order to represent a general FRF between force and response. (In the shaker systems this is typically an FRF between shaker voltage and the acceleration at the control accelerometers.) First, the FRF, $\boldsymbol{H}_{XF}(\omega)$, is decomposed using the singular value decomposition (SVD). In this derivation, it is assumed there are n outputs and d inputs where $d<n$.

$$\boldsymbol{H}_{XF}(\omega) = \boldsymbol{U}\boldsymbol{\Sigma}\boldsymbol{V}^{\boldsymbol{T}} \tag{16}$$

Here, $\boldsymbol{\Sigma}$ is a matrix containing the singular values of the decomposition as shown in Eq. (17).

$$\boldsymbol{\Sigma} = \begin{bmatrix} \sigma_1 & 0 & 0 \\ 0 & . & 0 \\ 0 & 0 & \sigma_d \end{bmatrix} \tag{17}$$

As a property of the SVD, the singular values are ordered by magnitude with the largest singular value being σ_1. Next, we define our condition number, c_i, for each singular value as follows.

$$c_i = \frac{\sigma_i}{\sigma_1} \tag{18}$$

With a threshold value defined, c_{th}, the index k is found by satisfying the condition below.

$$c_k > c_{\text{th}} > c_{k+1} \tag{19}$$

Then, a truncated k rank approximation of the pseudoinverse FRF is computed using the following.

$$\boldsymbol{H}^{+}_{XF}(\omega) = \sum_{i=1}^{k} \frac{1}{\sigma_i} \boldsymbol{V}_{\boldsymbol{i}} \boldsymbol{U}_{\boldsymbol{i}}^{\boldsymbol{T}} \tag{20}$$

Simulation Results with Condition Number Threshold

In order to see whether the MIMO tests could be predicted using simulations, each physical experiment presented in Table 3 was repeated in simulation with the threshold and without the threshold. A condition number threshold of 0.05 was used in simulation and experimental results. Table 6 presents the errors for each configuration in the format of *Simulation without Threshold / Simulation with Threshold / Physical Experiment*.

For all three configurations, the errors on the plate and stool are much more similar between the physical test and simulation when a condition number threshold of 0.05 is implemented. The simulations seem to do a reasonable job of predicting the success of a MIMO test, although there is some error in the predictions because the roving hammer FRF does not account for the shaker's dynamics.

The threshold affects the accuracy of the simulation by changing the input forces applied to the system. In Eq. (20) one can see that small values of σ_i can dramatically increase the magnitude of $\boldsymbol{H}^{+}_{XF}(\omega)$. If a large magnitude $\boldsymbol{H}^{+}_{XF}(\omega)$ is then used when computing the forces, the magnitude of the forcing input, $\boldsymbol{S}_{FF,est}(\omega)$, will also increase. In the experiments presented in this work, the control software was often unable to perform the desired test if the condition threshold was too low, because the forces needed were beyond the limits of the shakers. This case study shows that condition number thresholds can have a significant effect on a MIMO test and should be used in simulation if they will be used in the actual test.

Conclusions

This paper investigated the influence of impedance on the ability to reconstruct a random vibration environment for a component by controlling to accelerometers only on a transmission simulator that the component is attached to. A derivation showed that error in reconstructing an environment using the Transmission Simulator IMMAT method comes from two sources: 1.) a limit in the number of modal degrees

Table 6 Reconstruction accuracy error for the three configurations tested (Simulation without Threshold / Simulation with Threshold / Physical Experiment)

Assembly	Plate Error 100–5000 Hz (dB)	Stool Error 100–5000 Hz (dB)
Configuration A	2.7 / 4.7 / 7.7	19.2 / 18.4 / 16.3
Configuration B	3.2 / 7.7 / 7.5	20.9 / 17.2 / 12.1
Configuration C	2.9 / 10.4 / 9.3	28.4 / 13.5 / 12.5

of freedom of the TS that can be controlled due to a limited number of shakers, 2.) differences in the transmissibility of the tested assembly between the laboratory and the actual environment of interest. The latter affects how errors at the control accelerometers propagate to other places of interest on the structure. Several case studies were presented to explore the relative importance of these sources.

The results suggest a few interesting conclusions. First, Configuration A-2 showed that, if the impedance can be matched very closely between test and the true environment, that one can obtain very accurate results with relatively little difficulty. However, when even the best configuration available is quite far from the true flight boundary condition (e.g. Configuration C), then it seems to be much more important to limit the number of modes active in the transmission simulator for a fixed set of shakers rather than to try to match the flight boundary condition a little more closely. Specifically, while Configuration C included more of the vehicle, and presumably a closer match in impedance or transmissibility, worse results were obtained when using that Configuration as compared to Configurations A and B, presumably because those configurations had far fewer active modes. The mass-spring case studies clearly illustrated cases where the transmission simulator could be controlled at low frequencies, because the number of modes active was less than or equal to the number of shakers. At higher frequencies the shakers could not reproduce the environment precisely, and so they matched it at a few points on the structure and this might lead to significant errors at other points depending on the transmissibility of the system.

Lastly, to improve upon the ability of simulations to predict the results of an actual MIMO tests, a condition number threshold was implemented. This approach decreased the magnitude of the inverted FRF thereby also limiting the amplitude of the forcing input, similar to what is done in real MIMO tests. Comparing the error metrics between simulation and physical test, the simulations with the threshold implementation were consistently more predictive of the physical test.

Appendix: Shaker Selection Algorithm

Prior to performing any test, it is helpful to have a means of ensuring that the shaker locations used are adequate. The theory just presented shows how the spectra obtained in a MIMO test are related to the FRFs of the system of interest. Those FRFs can be created from a finite element model or measured experimentally; in this work we take the latter approach as detailed later.

The iterative shaker placement algorithm from [26] was adapted to find the shakers locations used in this work. First, the average dB difference of two ASDs for all relevant accelerometer channels at a frequency line is computed using Eq. (14). After computing an error value for each frequency line, a final metric is computed using Eq. (15). This final error number represents the average dB error across all accelerometers and frequency line. A low error metric communicates a successful reconstruction test and will be used moving forward to compare various tests. With the error metric defined, the shaker location algorithm used in this work is as follows:

1) Start with a pool of all possible forcing input locations from the roving hammer test of the component
2) Simulate the MIMO response for each forcing input location in the remaining pool (controlling to the eight plate accelerometers)
3) Identify the forcing input location that produces the lowest error on the controlled DOF (plate accelerometers). Add that input location to the set of chosen forcing locations and remove from the pool of possible locations.
4) Repeat steps 2–4 with the kept forcing input location/s from the previous iterations plus each candidate location and again keep the best candidate location until the number of desired shakers is reached.

The optimization was terminated once it determined the six best shaker locations. The error metric in Eq. (15) was also used in the results that follow to provide a measure of how successful a particular test was in recreating the desired environment.

Acknowledgements The authors gratefully acknowledge the Department of Energy's Kansas City National Security Campus, operated by Honeywell Federal Manufacturing & Technologies LLC, for funding this work under contract number DE-NA0002839.

Data Availability The flight data presented in this paper is available by request from the authors, pending clearance from the research sponsor. The simulation data from the simple spring mass systems can be shared upon request.

Declarations

Conflict of Interest The authors declare that there are no conflicts of interest.

References

1. Piersol A (1965) The development of vibration test specifications for flight vehicle components. J Sound Vib 88–115. https://doi.org/10.1016/0022-460X(66)90156-8
2. National Aeronautics and Space Administration (2003) "Force Limited Vibration Testing," NASA-HDBK-7004B. [Online]. Available: http://standards.nasa.gov. Accessed 31 Jan 2003
3. Paripovic J, Mayes RL (2021) Reproducing a Component Field Environment on a Six Degree-of-Freedom Shaker. In: Linderholt A, Allen M, D'Ambrogio W (Eds) Dynamic Substructures, Volume 4. Springer International Publishing, Cham, pp. 73–78. https://doi.org/10.1007/978-3-030-47630-4_6

4. Daborn PM, Roberts C, Ewins DJ, Ind PR (2014) "Next-generation random vibration tests," presented at the 32nd IMAC Conference and Exposition on Structural Dynamics, 2014, February 3, 2014 - February 6, 2014, vol. 8, pp. 397–410. https://doi.org/10.1007/978-3-319-04774-4_37
5. Mayes RL, Rohe DP (2016) Physical vibration simulation of an acoustic environment with six shakers on an industrial structure. In: Brandt A, Singhal R (eds) Shock & vibration, aircraft/aerospace, energy harvesting, acoustics & optics, vol 9. Conference proceedings of the society for experimental mechanics series. Springer, Cham. https://doi.org/10.1007/978-3-319-30087-0_4
6. Schultz R, Nelson G (2023) Techniques for modifying MIMO random vibration specifications. In: Walber C, Stefanski M, Harvie J (eds) Sensors and instrumentation, aircraft/aerospace and dynamic environments testing, vol 7. Conference proceedings of the society for experimental mechanics series. Springer, Cham. https://doi.org/10.1007/978-3-031-05415-0_7
7. Beale C, Schultz R, Smith C, Walsh T (2023) Degree of freedom selection approaches for MIMO vibration test design. In: Allen M, Davaria S, Davis RB (eds) Special topics in structural dynamics & experimental techniques, vol 5. Conference Proceedings of the society for experimental mechanics series. Springer, Cham. https://doi.org/10.1007/978-3-031-05405-1_10
8. Schultz' R, Avitabile P (n.d.) Application of an automatic constraint shape selection algorithm for input estimation. SAND2019-12628C, Sandia National Laboratories, Albuquerque, NM. https://www.osti.gov/servlets/purl/1642862
9. Schumann C, Allen MS, Tuman M, DeLima W, Dodgen E (2021) Transmission Simulator Based MIMO Response Reconstruction. Exp Tech. https://doi.org/10.1007/s40799-021-00454-4
10. Rohe DP, Schultz RA, Schoenherr TF, Skousen TJ, Jones RJ (2020) Comparison of multi-axis testing of the BARC structure with varying boundary conditions. In: Walber C, Walter P, Seidlitz S (eds) Sensors and instrumentation, aircraft/aerospace, energy harvesting & dynamic environments testing, Vol 7. Conference proceedings of the society for experimental mechanics series. Springer, Cham. https://doi.org/10.1007/978-3-030-12676-6_17
11. Jankowski K, Sedillo H, Takeshita A, Barba J, Bouma A, Abdelkefi A (2022) Impacts of test fixture connections of the BARC structure on its dynamical responses. In: Walber C, Stefanski M, Seidlitz S (eds) Sensors and instrumentation, aircraft/aerospace, energy harvesting & dynamic environments testing, vol 7. Conference proceedings of the society for experimental mechanics series. Springer, Cham. https://doi.org/10.1007/978-3-030-75988-9_13
12. Taylor CJ (2020) Using transfer path analysis and frequency based substructuring to develop a robust vibration laboratory dynamic test fixture design process. M.S. Thesis, Michigan Technological University, Houghton, MI
13. Reyes JM, Avitabile Peter (2018) "Force Customization to Neutralize Fixture-Test Article Dynamic Interaction," presented at the 38th International Modal Analysis Conference (IMAC XXXVI), Orlando, FL, 2018
14. Pacini BR, Kuether RJ, Roettgen DR (2022) Shaker-structure interaction modeling and analysis for nonlinear force appropriation testing. Mech Syst Signal Process 162:108000 https://doi.org/10.1016/j.ymssp.2021.108000
15. Dumont M, Cook A, Kinsley N (2016) Acceleration measurement optimization: mounting considerations and sensor mass effect. In: Topics in modal analysis & testing, Volume 10, Cham, pp. 61–71. https://doi.org/10.1007/978-3-319-30249-2_4
16. Scharton TD (1997) Force limited vibration testing monograph. NASA Technical Report, RP-1403
17. Segalman DJ et al. (2009) Handbook on Dynamics of Jointed Structures. Sandia National Laboratories, Albuquerque, NM 87185
18. Roettgen DR, Allen MS (2017) Nonlinear characterization of a bolted, industrial structure using a modal framework. Mech Syst Signal Process 84:152–170. https://doi.org/10.1016/j.ymssp.2015.11.010
19. Van Fossen T, Napolitano K (2021) An Acceleration-Based Approach to Force Limiting a Random Vibration Test. In: Epp DS (eds) Special Topics in Structural Dynamics & Experimental Techniques, vol 5. Conference Proceedings of the Society for Experimental Mechanics Series. Springer, Cham. https://doi.org/10.1007/978-3-030-47709-7_29
20. Larsen W, Schultz R, Zwink B (2023) Multi-shaker testing at the component level. In: Walber C, Stefanski M, Harvie J (eds) Sensors and instrumentation, aircraft/aerospace and dynamic environments testing, vol 7. Conference proceedings of the society for experimental mechanics series. Springer, Cham. https://doi.org/10.1007/978-3-031-05415-0_11
21. Tuman MJ, Schumann CA, Allen MS, Delima WJ, Dodgen E (2022) Investigation of transmission simulator-based response reconstruction accuracy. In: Walber C, Stefanski M, Seidlitz S (eds) Sensors and instrumentation, aircraft/aerospace, energy harvesting & dynamic environments testing, vol 7. Conference proceedings of the society for experimental mechanics series. Springer, Cham. https://doi.org/10.1007/978-3-030-75988-9_4
22. Schumann CA, Allen MS, DeLima WJ, Dodgen E (2021) Transmission simulator based MIMO response reconstruction for vehicle subcomponents. In: Epp DS (eds) Special topics in structural dynamics & experimental techniques, vol 5. Conference proceedings of the society for experimental mechanics series. Springer, Cham. https://doi.org/10.1007/978-3-030-47709-7_18
23. Mayes R, Ankers L, Daborn P, Moulder T, Ind P (2020) Optimization of Shaker Locations for Multiple Shaker Environmental Testing. Exp Tech 44(3):283–297. https://doi.org/10.1007/s40799-019-00347-7
24. Schultz R (2021) Vibration test design with integrated shaker electro-mechanical models. In: Linderholt A, Allen M, D'Ambrogio W (eds) Dynamic substructures, vol 4. Conference proceedings of the society for experimental mechanics series. Springer, Cham. https://doi.org/10.1007/978-3-030-47630-4_5